THE JOURNAL OF PHYSICAL CHEMISTRY C

pubs.acs.org/JPCC

Article

Role of Rare Earth Ions in the Prevention of Dealumination of Zeolite Y for Fluid Cracking Catalysts

Jaap N. Louwen, Stanislav Simko, Katarina Stanciakova, Rosa E. Bulo, Bert M. Weckhuysen, and Eelco T. C. Vogt*

Cite This: J. Phys. Chem. C 2020, 124, 4626−4636

Read Online

ACCESS | Metrics & More | Article Recommendations | Supporting Information

ABSTRACT: In this work, we use quantum-mechanical calculations to examine a number of possible dealumination routes in a model reminiscent of a commercial Y zeolite (Si/Al ratio of 3) as used in fluid catalytic cracking. First, we determine the distribution of Al over the zeolite lattice. The thermodynamically most stable distribution found in our calculations does not match the aluminum distribution found experimentally with NMR. We then describe the design of a periodic structure model to better fit the experimental distribution for zeolite Y with a Si/Al ratio of 3. This new model is used to determine the mechanism of dealumination in the absence and presence of stabilizing La^{3+} ions. It was found that the dealumination pathways with La^{3+} present in this model lead to higher activation energies, supporting a stabilizing effect of rare earth ions on the dealumination. The local environment (with both Brønsted and Lewis acid sites) has a large effect on the transition states and intermediates. While the local environment destabilizes pathways that involve protonation of oxygen atoms near another Brønsted acid site, it reduces the barriers of other pathways by coordinating newly formed OH groups in the transition states. These findings imply that the realistic aluminum distributions provided by our model are a prerequisite for this type of study.

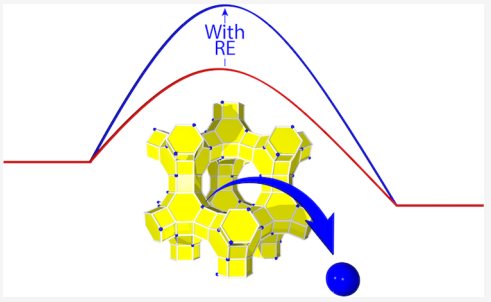

INTRODUCTION

Fluid catalytic cracking (FCC) is the main conversion process in the oil refinery, producing a large part of the world's gasoline, as well as base chemicals, such as propylene.[1] The FCC process was developed in the early 1940s as the successor of the fixed-bed Houdry cracking process, which used clay-based catalysts, and has seen a number of improvements over the years. One of the major innovations was the introduction of microporous zeolites to the catalyst in the early 1960s, following the work of Milton and Breck, who discovered a number of synthetic zeolites at Union Carbide, see, e.g., ref 2. Synthetic zeolites provide a considerable increase in cracking activity as well as gasoline selectivity over amorphous catalysts. However, the process conditions (cracking at around 538 °C, regeneration at 700 °C) are so severe that the zeolites eventually collapse.

Already in the early 1960s, Plank and Rosinski[3] observed a large positive effect of using rare earth (RE)-exchanged zeolites compared to amorphous silica−alumina or Na-exchanged zeolite Y. Li and Rees[4] showed that the temperature at which the zeolite structure collapses shifts toward higher temperatures for RE-exchanged zeolite Y. Rabo et al.[5] showed that clusters of RE-hydroxide species are located inside the sodalite cages, similar to observations by Lee and Rees.[6] Various authors investigated the stabilizing effect of RE in zeolite Y in the 1960s and 1970s. Their IR and NMR data seem to indicate that a larger portion of lattice Al atoms remains in their framework position. It is to be noted that the Breck−Flanigen relation[7] explaining the shrinkage of the zeolite lattice upon dealumination (the Si−O bond is shorter than the Al−O bond) is not valid in the case of RE-exchanged zeolite Y.[8] The presence of RE seems to induce a lattice expansion. Van Bokhoven et al. have explained this effect.[9] The majority of the authors seem to believe that the RE ions move into the I′-ion-exchange site, and from there, they exert a stabilizing effect by electrostatic interaction. Schüßler et al. examined the speciation and localization of La ions in the zeolite structure, among others with periodic density functional theory (DFT) calculations.[10] These authors place the majority of the RE species in multinuclear hydroxide-bridged moieties, essentially similar to Rabo's observations. Some of the RE ions, according to the authors, are located in the supercages in the II site and are able to activate hydrocarbons. Noda et al., based on cluster DFT calculations, offer a similar explanation for the increased activity.[11] They claim that OH sites are removed from hexagonal prism- and sodalite cage locations, whereas stronger Brønsted acid OH sites are formed in the supercages because the small highly charged RE ions induce a polarization

Received: December 27, 2019
Revised: January 30, 2020
Published: February 5, 2020

https://dx.doi.org/10.1021/acs.jpcc.9b11956
J. Phys. Chem. C 2020, 124, 4626−4636

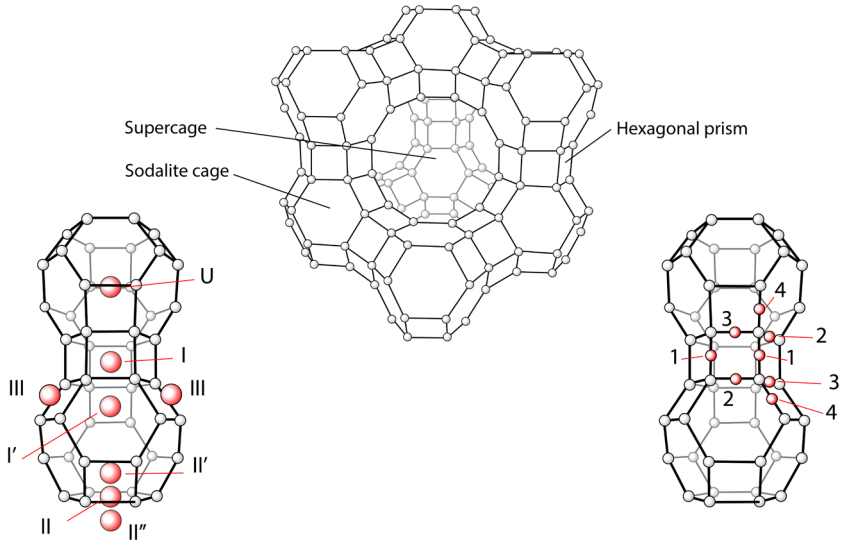

Figure 1. Schematic description of the lattice of zeolite FAU with RE ion-exchange positions I–III (left) and oxygen positions 1–4 (right).

effect. Although both works offer a plausible explanation for the increased activity, they do not explain the enhanced framework stability. Silaghi et al. investigated dealumination pathways for isolated Al atoms in zeolites MOR, CHA, FAU, and MFI.[12] In this work, we build a realistic model for zeolite Y with a higher Al content, and we elucidate the effect of a La ion (in the form of a La^{3+} ion) on the dealumination pathways.

COMPUTATIONAL DETAILS

We computed all possible dealumination pathways (in the absence and presence of lanthanum) for the three Al sites in our final zeolite model that are located closest to the lanthanum ion. The calculations were performed with the Quickstep module of the CP2K program[13−17] set, version 4.1, using the Perdew–Burke–Ernzerhof (PBE) density functional[18] and the MOLOPT-DZVP basis set[19] with Goedecker–Teter–Hutter (GTH) pseudopotentials.[20−22] The rationale for using this potential set, and for not using dispersion corrections, is explained in ref 23. CP2K employs the FFTW3 library for fast Fourier transform.[24] The basis set and pseudopotentials used are the applicable ones distributed with the CP2K program, with the exception of the basis set for La. For this, we used the set made publicly available by Ling.[25] Program settings were default, apart from the cutoff energy for the finest grid level, which was increased from its default value of 280–700 Ry units. Furthermore, the target accuracy for self-consistent field (SCF) was increased from 10^{-5} to 10^{-7} charge units. Since the atomistic model is rather large, only the Γ-point was computed; no integration over the Brillouin zone was performed. The CP2K calculations were performed on the former Irish national supercomputer Fionn with support from the PaRtnership for Advanced Computing in Europe-Distributed European Computing Initiative (PRACE-DECI).

TRANSITION-STATE OPTIMIZATION

All (final) transition states were computed by means of the dimer method.[26] To generate appropriate initial guesses for the transition-state optimization, we performed constrained geometry optimizations when possible and used the climbing image nudged elastic band (CI-NEB) method[27] otherwise. We decreased the CP2K convergence limit for the direction of the smallest curvature in the dimer method from its default value of 0.08 rad (5°) to 0.01 or even 0.005 rad.

BENCHMARKS OF THE LANTHANUM DESCRIPTION

In the version of CP2K used in this study (4.1), the relativistic corrections for valence electrons have been disabled. Valence electrons are affected by relativistic effects directly only if their orbitals penetrate deeply into the core or indirectly because the properly relativistically treated core is more contracted than a nonrelativistically computed one and will therefore shield the valence electrons more effectively from the nuclear charge. Both effects can be largely taken care of by the pseudopotentials generally used in solid-state DFT codes. For La, we explicitly treat only the outermost 11 electrons of the 57 (these are $5s^2$, $5p^6$, $6s^2$, $5d^1$). We therefore assume that the (relativistically derived) pseudopotential will give us sufficiently accurate results even without further relativistic corrections on the valence orbitals.

To investigate this assumption, we benchmarked CP2K results for La-containing solids against the experiment and the results of a variety of programs (CP2K,[13−17] VASP,[28] Quantum Espresso,[29] BAND,[30−34] CRYSTAL2003,[35] and CASTEP[36]) both from the literature and computed by ourselves. The results of this benchmark can be found in the Supporting Information (SI) (Tables S1–S7 and accompanying text). On the basis of comparisons of the structures of A-La_2O_3, C-La_2O_3, $La(OH)_3$, $LaPO_4$, and an all-electron fully relativistic calculation for a La atom, we conclude that the results of using CP2K on La-containing materials using the MOLOPT-DZVP basis set and the GTH pseudopotential are acceptable.

ATOMISTIC ZEOLITE Y MODEL

Zeolite Y crystallizes in the faujasite (FAU) framework structure, a cubic structure in the space group $Fd\bar{3}m$ (space group 227, generally used in the second setting). The pure silica polymorph of this framework contains 576 atoms in the unit cell (192 T-sites). Introducing Al, protons, water, and La into the structure at realistic ratios, the contents of the unit cell quickly grow to well over 600. Fortunately, the space group is

https://dx.doi.org/10.1021/acs.jpcc.9b11956
J. Phys. Chem. C 2020, 124, 4626–4636

face-centered, which implies that the problem can be simplified by applying a rhombohedral primitive unit cell that is only one quarter of the size of the cubic cell, and contains only 48 T-sites.[37] We always imposed the constraints that A = B = C and $\alpha = \beta = \gamma = 60°$, ensuring that the results can be related to the cubic cell, and will report the results of unit cell optimizations in terms of the more familiar cubic cell axes. A realistic ratio of Si to Al atoms for zeolite Y in FCC is 3 (the molar ratio of the oxides, SiO_2/Al_2O_3, is 6 in that case). This corresponds to a total of 12 Al atoms in the rhombohedral cell. The initial step in the building of the model was to calculate the optimized structure (atom positions and lattice) of the all-silica analogue. Subsequently, Al atoms were placed at different T-sites, and for the resulting structures, energies and NMR spectra were compared.

RESULTS AND DISCUSSION

In the first part of this work, we describe the development of a model of zeolite Y that optimally matches the catalyst used in the relevant experiments, while in the second part we use the model to determine the dealumination pathways in the absence and presence of a lanthanum ion.

ZEOLITE Y MODEL DEVELOPMENT

We first determine the most energetically favorable atomistic model for zeolite Y with a Si/Al ratio of 3. We subsequently obtain the model that best matches experimental NMR data, using simulated annealing.

THERMODYNAMIC OPTIMIZATION

Optimization of the all-silica zeolite Y model yielded a unit cell of 24.5291 Å, approximately 1.4% larger than expected from the Breck–Flanigen relationship (which would yield 24.19 Å).[7] The position of the first Al atom in the structure is not important, since all tetrahedral sites in the all-silica structure are equivalent. Each T-atom has four different oxygen atoms linked to it, from which we have to select one to place the charge-compensating proton. It appears that site O1, in the side of the hexagonal prism (Figure 1), is slightly more favored than the other three positions. We therefore use the O1 position for proton placement in all further structures. As is clear from Table 1, the unit cell expands a little with the introduction of Al (and a proton), as is expected from the relevant experiments.[7,38]

Table 1. Relative Protonation Energies for the Four Oxygen Atoms Connected to the First Al Atom

H on	relative energy (kcal/mol)	UCS (Å)
O1	0.00	24.5621
O2	2.31	24.5628
O3	0.86	24.5609
O4	2.12	24.5576

Placing an additional Al atom destroys the symmetry of the lattice. This leaves us with 47 possibilities for placing the second aluminum atom. We investigated the eight possibilities that are two or three bonds away (Loewenstein's rule[39] forbids Al–O–Al linkages). Surprisingly, the most favorable position by far is the opposite position in the same four-membered-ring in the hexagonal prism that bears the initial Al (see Table 2 and Figure 2).

Table 2. Relative Energies for Placing a Second Al Atom (for the Positions, We Refer to Figure 2)

second Al on	relative energy (kcal/mol)	UCS (Å)
1	0.00	24.5991
2	8.15	24.6011
3	7.97	24.5973
4	8.44	24.5998
5	6.76	24.6010
6	6.71	24.6002
7	6.72	24.6012
8	5.36	24.5966

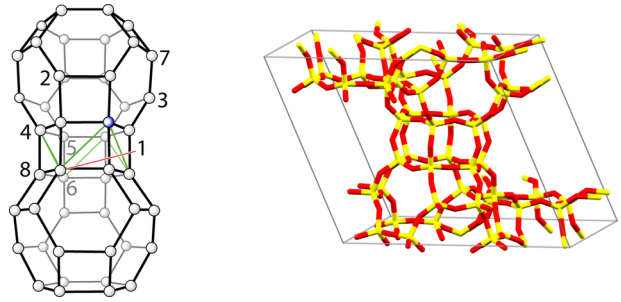

Figure 2. Left: possible Al lattice positions available after the first insertion into the lattice; the green lines show the "zigzag" substitution pattern that emerges as the energetically most favorable. Right: primitive unit cell with all atoms for comparison.

Dempsey's rule,[40] based on electrostatic arguments, would prescribe that the second Al is as far away as possible from the first, but that apparently does not hold. Schröder and Sauer,[41] using METAPOCS[42] forcefield calculations, observed a similar effect, with next nearest neighbors in the four-ring more stable by 7–9.5 kcal/mol compared to larger distances. They find a slightly more stable position (by 1.8 kcal/mol) for a second Al atom in the sodalite cage (position 2 in Figure 2) rather than the hexagonal prism.

When placing the third Al atom, the position across the four-ring in the hexagonal prism (position 4 in Figure 2) is the most favorable out of the fifteen possible sites in the vicinity of the original atoms, so a V-shape is formed. Other options, e.g., placing three atoms in one six-ring (obeying Loewenstein's rule), yield a substantially less favorable energy (+17.04 kcal/mol).

A number of options for placing the fourth atom are detailed in the Supporting Information. Again, the continuation of the zigzag order filling up the hexagonal prism gives the lowest energy.

Placing more than four atoms in the structure quickly becomes an overwhelming problem, so only a limited number of possibilities were explored. For placing six atoms, it is energetically more favorable by 9.53 kcal/mol to have the six atoms in one hexagonal prism (in the zigzag pattern) rather than spreading them equally over two different prisms (using the V-shaped distribution found for the first three Al).

When placing 12 Al atoms, a distribution with two times six atoms in the separate prisms is more favorable by 12.43 kcal/mol than a distribution with four times three atoms in four separate prisms. Placing 12 Al atoms in the primitive unit cell constitutes a Si/Al ratio of 3.

It thus appears from this study that it is thermodynamically favorable to place as many Al atoms in hexagonal prisms as Loewenstein's rule would allow. This would imply that the

https://dx.doi.org/10.1021/acs.jpcc.9b11956
J. Phys. Chem. C 2020, 124, 4626–4636

majority of the Si atoms would have either zero or three Al neighbors. However, this is not what experimental evidence from ^{29}Si NMR suggests.

MATCHING EXPERIMENTAL DATA

Klinowski et al.[43] and Melchior et al.[44] studied the coordination environment of Si in zeolite NaX and NaY with ^{29}Si NMR. The latter report is more extensive. Melchior et al. measured the Si coordination in a range of zeolite Y samples with different Si/Al ratios. One of the samples had a ratio of 2.97 (SiO_2/Al_2O_3 5.93). Klinowski et al. measured a sample with a ratio of 2.69 (SiO_2/Al_2O_3 5.38); these are closest to our model with SiO_2/Al_2O_3 = 6.

By means of simulated annealing, we identified the placement of 12 Al among the 48 positions in the rhombohedral cell that gave the best match (smallest sum of squares of differences) in occupations with the zeolite of silica/alumina molar ratio (SAR, i.e., SiO_2/Al_2O_3) 5.93. No violations of Loewenstein's rule were allowed (some exceptions to Loewenstein's rule are documented, but they concern either exotic materials or theoretical structures[45−47]). The simulated annealing procedure was carried out over a large number of steps and repeated several times. Each time the same solution was obtained. The detailed results are presented in Table S12 in the Supporting Information.

The total Si(*n*Al) distribution found is in good agreement with Melchior et al. and in reasonable agreement with Klinowski et al. (who measured a sample of lower SAR). The relative energies for the structure with 12 Al atoms in the lattice obtained in this way can be compared to the two 12-Al structures that were described above (Table 3).

Table 3. Relative Energies for Different Options for Placing 12 Al Atoms in the Unit Cell

distribution of 12 Al	relative energy (kcal/mol)	UCS (Å)
6/6/0/0 over four prisms	0.00	25.0235
3/3/3/3 over four prisms	12.43	25.0234
matching ^{29}Si NMR data	29.96	25.0162

The NMR-based Al distribution is obviously quite different from a distribution that minimizes the total energy. Al is not distributed in a way that minimizes lattice energy.

The Al distribution is set during the crystallization, in which Na^+, and not H^+, is the counterion. In the Supporting Information, we present a brief study in which the counterions in the structures reported in Table 2 are replaced by Na^+, or removed altogether. In both cases, the ranking of the possible positions is completely different (Table S8). This implies that the hardness of the counterion is important in determining the relative energies of different Al distributions. The harder the counterion, the more charge resides on the Al defects in the silicon lattice, and the stronger the electrostatic interaction between defects becomes. This of course influences the optimal distribution, and again, Al appears not to be distributed in a way that minimizes lattice energy.

We will therefore use the distribution derived from NMR for our further calculations. The distribution of Al in the lattice should not change during ion exchange replacing the Na^+ with H^+, which is why the distributions found by Klinowski et al. and Melchior et al.[43,44] are applicable to our system. The CP2K optimized coordinates for the NMR-based distribution are given in the Supporting Information (Table S12).

The NMR-matched Al distribution leads to a unit cell featuring one hexagonal prism with two Al, one with four Al, and two with three Al. From the latter two, we limit our study to the hexagonal prism with two Al in the bottom six-ring, separated by two Si T-sites, and one in the top six-ring. The distribution is illustrated in Figure 3.

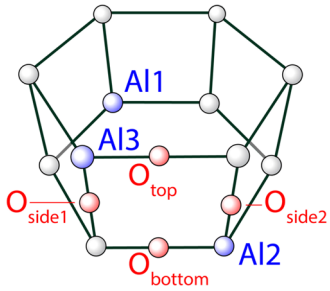

Figure 3. Realistic Al distribution in the hexagonal prism of FAU-zeolite based on NMR data.

RE-POSITION AND COORDINATION

To find the optimal position for a La^{3+} ion in the zeolite framework, one needs to start from a zeolite structure where all three Brønsted protons are removed from the hexagonal prism to maintain a charge−neutral system. A number of possible positions for the La^{3+} ion were examined, and their relative energies are presented in Table 4. For comparison, the reference energy for a water molecule is that of a molecule in the gas phase.

Table 4. Relative Energies for the Different Placement Options for a La^{3+} Ion

position	energy (kcal/mol)
bare La^{3+} at the I position within the hexagonal prism	0.0
La^{3+} within the hexagonal prism with a molecule of water coordinated	−13.0
A bare La^{3+} at the I′ position just outside the hexagonal prism (Figure 1)	+18.4
La^{3+} at the I′ position with one H_2O coordinated	−11.8
La^{3+} at the I′ position with two H_2O coordinated	−38.9
La^{3+} at the I′ position with three H_2O coordinated	−58.9
La^{3+} at the I′ position with four H_2O coordinated	−66.0

This implies that, in the absence of water, the La^{3+} will be localized in the I position in the center of the hexagonal prism. This is indeed observed in structure elucidations of dehydrated samples.[48] Since we are concerned with the dealumination during steaming, we need to account for the role of water. When water is present, the most likely position is in site I′, with the La^{3+} coordinated with three water molecules. While the addition of a fourth water molecule is energetically favorable, the energy gain is much less than that for the addition of the second and third molecules. Moreover, the fourth water molecule would severely restrict the thermal movement of the other three under dynamic conditions. Moving the bare La^{3+} from site I to site I′ has a computed activation barrier of 18.6 kcal/mol. In the presence of one water molecule, the activation barrier to move the La^{3+} from site I to site I′ is only 5 kcal/mol. The overall move is slightly endothermic (1.2 kcal/mol), but the presence of additional

https://dx.doi.org/10.1021/acs.jpcc.9b11956
J. Phys. Chem. C 2020, 124, 4626−4636

water in the sodalite cage will lead to the formation of more stable structures with two and three water molecules coordinated. When one or two water molecules were taken away from three water molecules coordinated to the La^{3+} ion and placed elsewhere in the sodalite cage, either these drifted back to the La^{3+} ion or, if there was a sufficiently large energy barrier to prevent that, the resulting structure had a higher energy.

The structure with the La^{3+} ion at the I′ position with three water molecules coordinated is stable with respect to protonation of the framework. We investigated removing one of the protons from one of the available water molecules and placing this proton on different oxygen atoms of the adjacent prism, as indicated in Figure 3. However, this always leads to less stable structures. Table 5 presents the computed relative energies.

Table 5. Relative Energies for Moving a Proton to Different Oxygen Atoms[a]

structure	energy (kcal/mol)
La^{3+} at I′ + 3 water	0.0
proton moved to	
O_{bottom}	unstable
O_{side1}	+23.0
O_{side2}	+18.3
O_{top}	+13.8

[a]The labeling of oxygen atoms is shown in Figure 3.

In the remaining part, we will thus work with the La^{3+} in the I′ position coordinated with three water molecules.

DEALUMINATION ROUTE

In the next section, we will examine the dealumination of the FAU lattice for all three Al sites from the model above (Figure 3), in both the absence and presence of the La^{3+} ion. To understand the influence of additional Brønsted and Lewis acid sites, the results will be compared with the dealumination pathway for a zeolite Y model with a 47/1 Si/Al ratio (or SAR 94, i.e., an isolated Al site). As the dealumination proceeds, the newly coordinated basic hydroxyl groups at the reacting Al atom interact with the remaining Brønsted and Lewis acid sites. We expect this interaction to have profound effects on the energetics, yielding a pathway for dealumination that is very different from the pathway followed by an isolated Al site.

DEALUMINATION IN THE ABSENCE OF RE

The first step in the dealumination is the adsorption of a water molecule on Al. If sterically possible, we expect the water to coordinate to Al opposite the weakest bond, which is generally the bond to the protonated oxygen atom.[12] As noted above, O1 is the favored site for placing the proton of the Brønsted Al−O(H)−Si moiety, so to limit the number of possibilities, we have focused on dealumination routes that start in this way. We find that the water coordination is indeed the most favorable opposite O1, weakening the Al−O1 bond even further. For the remaining three steps of the dealumination pathways, there are many possibilities, some of which yield equivalent structures. We will use the following description. We start with the original location of the Al atom, using the numbering in Figure 3 (HY1, HY2, or HY3 for the RE-free system, or REY1, REY2, or REY3 for the RE-exchanged system). The adsorption of water to the Al atom is denoted "W". For this step, we calculate the adsorption energy only. This step is illustrated in Figure 4 for an isolated Al atom.

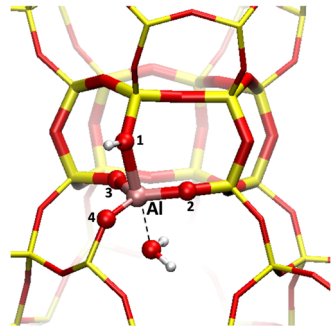

Figure 4. A single water molecule is chemisorbed to the Al site in the SAR = 94 zeolite (pathway HYW). Color coding: H = white, O = red, Al = pink.

The next step is the jump of a proton from adsorbed water to one of the remaining oxygen sites. This step is denoted "P*X*", with *X* being the number of respective oxygen atoms; using the numbering in these steps, both the reaction energy and the activation energies were calculated. Thus, a path up to this point could be HY1WP2. The steps are then repeated to calculate each possible dealumination pathway starting from the hydration at position 1 (Figure 5).

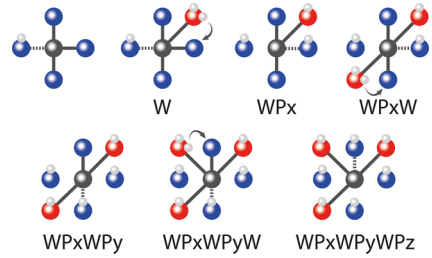

Figure 5. Schematic drawing of the steps in the dealumination pathway. Blue atoms represent oxygen atoms that are and remain connected to the zeolite framework through Si−O bonds. Red atoms represent oxygen atoms coming from water and are not connected to the framework.

ISOLATED AL SITE

We demonstrate the procedure for the special case of an isolated Al atom (which we call "HY"). For the first hydration ("W"), the sorption energy is −9.0 kcal/mol (Figure 4). There are three possibilities for the next step: WP2, WP3, and WP4. The activation energies for these steps are 27.1, 21.5, and 40.0 kcal/mol, respectively. The WP4 route yields activation energies that are substantially higher than the other possibilities in all seven pathway analyses, so WP4 will not play a significant role and will not be examined further. The WP3 route has the lowest activation energy and can be followed by either WP3WP2 or WP3WP4. These are essentially equivalent in activation energy (15.5 and 15.2 kcal/mol, respectively). Likewise, WP2 can be followed by WP2WP4 and WP2WP3. We find that the latter pathway leads to the same structure as WP3WP2. Overall, WP3WP2WP4 has the lowest maximum activation energy and is thus the minimum energy pathway (MEP) (Figure 6).

https://dx.doi.org/10.1021/acs.jpcc.9b11956
J. Phys. Chem. C 2020, 124, 4626−4636

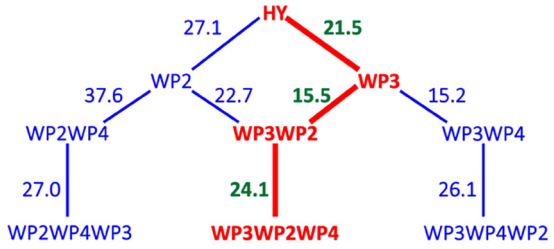

Figure 6. Activation energies for all possible pathways starting from a single Al site in the FAU lattice. WP2WP3 and WP3WP2 yield the same structure. WP3WP2WP4 is the minimum energy pathway.

The difference in activation energies between WP3WP2WP4 and WP3WP4WP2 may only be 2 kcal/mol, but the structures themselves are radically different. In WP3WP2WP4 (as well as in WP2WP4WP3), the $Al(OH)_3$ moiety is found inside the sodalite cage, whereas in WP3WP4WP2, it is found in the main cage. This is because the strain in the WP3WP4 transition state is partly resolved by pulling Al into the main cage. The full dealumination route for HY is illustrated in the Supporting Information (see Figures S6–S10 and the accompanying text).

EFFECT OF NEIGHBORING BRØNSTED AND LEWIS ACID SITES

Focusing on the model with a Si/Al ratio of 3 (SAR = 6), minimum energy pathways were determined for the dealumination of the three different aluminum sites (HY1, HY2, and HY3). These are compared to the route for the HY pathway in the unit cell with a single Al in Figure 7. The activation energies and reaction energies for all routes examined can be found in the Supporting Information (Figures S15–S20 and Tables S12–S15).

It is striking that the minimum energy pathway (MEP) is a different one for every site. For HY1, it is WP3WP2WP4 (as it was for the single Al in the SAR = 94 zeolite); for HY2, it is WP3WP4WP2; and for HY3, it is WP2WP3WP4. As we consistently find high activation energies for HY*x*WP4, no pathway starting with WP4 can be the MEP (and WP2WP3 leads to the same result as WP3WP2). Since WP3WP4WP2 leads to dislodged Al outside of the sodalite cage (like with the single site in the SAR = 94 zeolite), whereas the other pathways will bring it into the sodalite cage, the MEP of HY2 leads to a final result different from that of both HY1 and HY3 (and the single site of the previous section).

The highest activation energy encountered along the MEP is also significantly different: 19.7, 21.9, and 23.6 kcal/mol, respectively, for HY1, HY2, and HY3 (all lower than the 24.1 kcal/mol for the single site in the SAR = 94 zeolite).

It is thus clear that there are substantial differences between the three sites. Therefore, the local environment has a great influence on the dealumination energetics. Ideally, we should have done the calculations for all 12 Al sites in the SAR = 6 unit cell, but that was not possible within the (computer-)time available.

Without going through all pathways in detail, we will discuss some cases where the interaction with the lattice is strong to

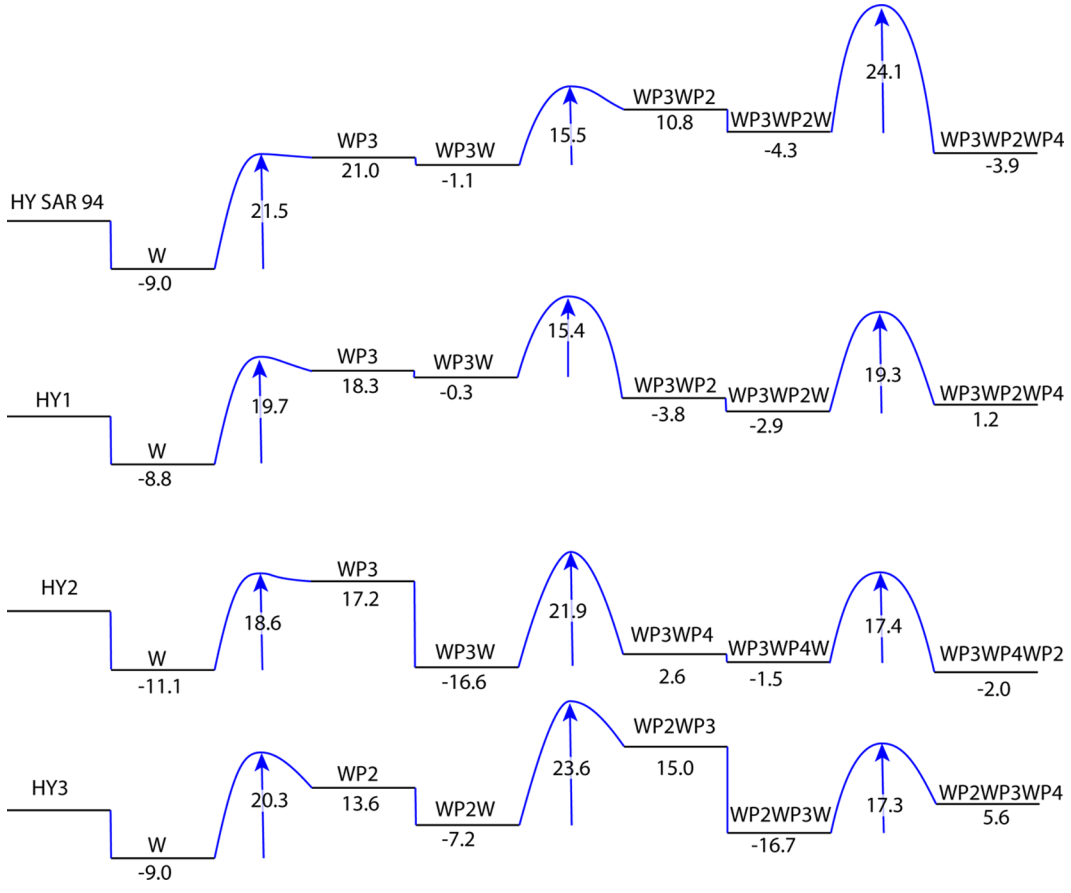

Figure 7. Minimum energy pathways for the SAR 94 HY model (top) and the HY1, HY2, and HY3 sites in the SAR6 model.

https://dx.doi.org/10.1021/acs.jpcc.9b11956
J. Phys. Chem. C 2020, 124, 4626–4636

show what may be expected along a dealumination pathway in a realistic HY zeolite.

For HY1, we find that in the transition state from HY1WP2W to HY1WP2WP3 (or HY1WP3WP2), the water molecule is closer to a Si in the lattice (1.81 Å) than to the Al (2.59 Å). In the HY1WP3WP2 structure, these distances are 1.89 and 1.95 Å; the OH has become bridging. The structures are shown in Figure 8.

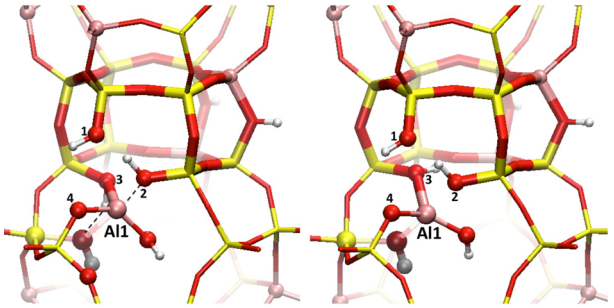

Figure 8. HY1WP2WP3 transition state (left) and the final HY1WP3WP2 structure (right).

The interaction between the hydroxyl group and the Si atom is driven by the Lewis acidity of the Si, which is part of an Al−O(H)−Si moiety. In HY1WP3WP2, the distance between Si and its "own" O(H) is 1.93 Å. In a manner of speaking, the Lewis acidity of this Si is borrowed from the Al in the Al−O(H)−Si moiety. Note that in this structure the Al−O3 bond is retained (distances: Al−O3 1.95 Å, Al−O2 2.01 Å). This is caused by the fact that the linkage between a hydroxyl and the lattice Si draws Al to the side of O3.

A similar bonding between a hydroxyl and a lattice atom occurs in the transition state to HY1WP2WP4 as well as in HY1WP2WP4 itself. In the transition state to HY1WP2WP4WP3, the hydroxyl temporarily latches on an Al in the lattice, which incidentally causes Al to move away from O4 (see the Figure S11, Supporting Information). In the lowest energy structure for HY1WP2WP4WP3 (equivalent to HY1WP3WP2WP4), the hydroxyl is again coordinated to the Si atom.

This is also observed in HY2WP2W, but in this case the OH connects with the same Si that O2 is attached to, resulting in two hydroxyl groups bridging between the same Si and Al (Figure S12).

Another feature worth mentioning is that in the structure of HY3WP3WP4, we find a water molecule attached to the partially dislodged Al. This is because a hydroxyl group of that Al has picked up a proton from an Al−O(H)−Si Brønsted site. The structure is shown in Figure S14. The O from which the proton originates is only visible in the image as the end of a stick; it is at 1.78 Å distance from the proton. This is a regular length for hydrogen bonding (the O−H bond length on the water moiety is 1.00 Å), which shows that the proton has been fully transferred, and we have a zwitterionic arrangement within the zeolite.

Another remarkable example of the environment effect can be found in the first reaction step of HY2 and HY3 (Figure S13). The HY2WP2 and HY2WP3 activation energies are 28.2 and 18.6 kcal/mol, while for HY3WP2 and HY3WP3 the values are 20.3 and 27.6 kcal/mol, respectively. At first sight, this appears hard to rationalize as HY2 and HY3 are opposite to each other in a four-membered face of the prism (Figure 3). However, the superficial symmetry is deceiving. The four-membered ring contains, apart from two (protonated) O1 atoms, an O2 connected to HY2 and an O3 connected to HY3. It appears that the O that gets preferentially protonated is the one farthest away from a neighboring Al. This suggests that pathways involving protonation of an oxygen atom near another Brønsted acid site are destabilized. The ordering of WP2 and WP3 activation energies for HY3 is different not only from HY2 but also from HY1 and the single site in the SAR = 94 zeolite. A contributing factor may be that the transition state for HY3WP2 is somewhat stabilized by coordination of the O of the dissociating water molecule to a Lewis acidic Si in the lattice (Si···O = 2.37 Å).

DEALUMINATION ROUTES IN THE PRESENCE OF RE

The introduction of a La^{3+} ion incurs the loss of three protons. As computed above, it is energetically the most favorable to have a $[La(H_2O)_3]^{3+}$ unit coordinated to the six-membered ring of the prism with two Al (sites REY1 and REY2) and no protons anywhere on the prism. This makes REY3 formally a site of negative charge, which has implications for its dealumination. We will therefore start with a discussion of

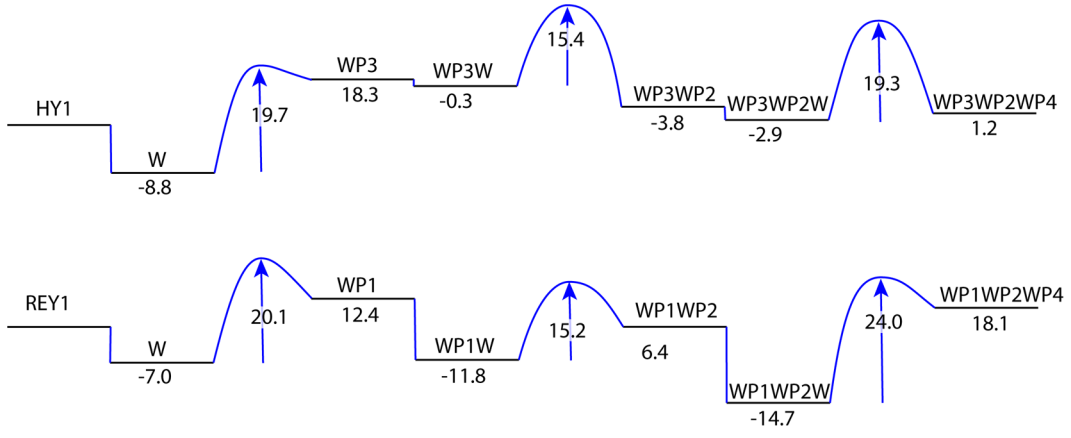

Figure 9. Minimum energy dealumination pathway for REY1 compared to HY1. The minimum energy pathway for the RE-exchanged material is 4.3 kcal/mol higher in activation energy.

https://dx.doi.org/10.1021/acs.jpcc.9b11956
J. Phys. Chem. C 2020, 124, 4626−4636

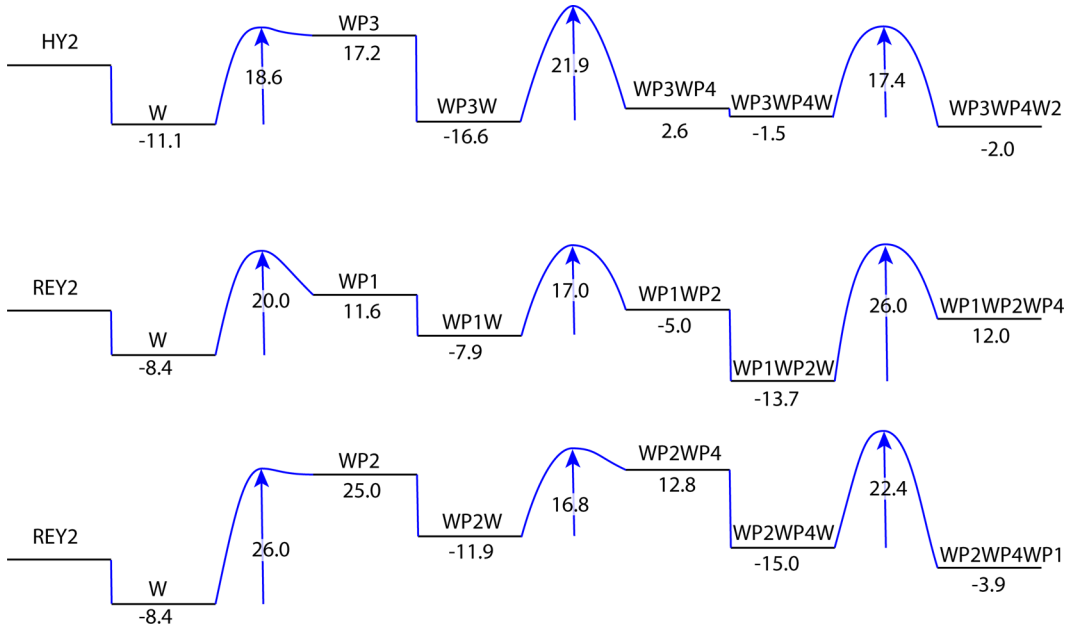

Figure 10. Minimum energy dealumination pathway for REY2 compared to HY2. There are two different minimum energy pathways that both feature 26.0 kcal/mol as the maximum activation energy. Both minimum energy pathways for the RE-exchanged material are 4.1 kcal/mol higher in energy compared to the HY2 pathway.

REY1 and REY2 for which the dealumination proceeds in a fairly straightforward manner.

In these two cases, the weakest Al−O bond is Al−O3 (as O3 is closer to the La^{3+} ion than O2 and therefore more strongly bound to it), so the first water molecule is sorbed opposite O3.

The minimum energy pathways for REY1 and REY2 are compared to the HY minimum energy pathway in Figures 9 and 10. With REY, WP3 is no longer the preferred first step, which is to be expected as O3 has taken over the role of O1 as the oxygen opposed to which water is sorbed. Also, in the presence of RE, we generally find larger activation energy barriers.

The REY3 site is different from all other sites. It does not have a proton associated with it and neither is any of its oxygen atoms coordinated to the La^{3+} ion, so it bears a formal negative charge. This implies that it is not possible to donate electrons from a water molecule, and indeed every attempt to make the site accept a water molecule led to instant rejection. Therefore, the REY3 site cannot be dealuminated in the same way as the other sites.

However, there are a number of viable dealumination pathways for REY3. They all require the donation of a proton to one of the oxygens surrounding it. One could imagine a pathway in which a proton hops from one of the three water molecules coordinated to the La^{3+} ion to one of the REY3 oxygens. This is not energetically favorable (+13.8 kcal/mol for the most favorable case, O3), but not impossible. We have initiated a pathway from the structure it would produce (dubbed REY3H). The minimum energy route for this pathway is REY3HWP1WP2WP4, with a maximum activation energy barrier of 29.7 kcal/mol. This makes REY3 the least prone to dealumination among all of the Al sites, with and without RE. All energies calculated for this route can be found in the SI.

Another possibility relies on the weak Lewis acidity of the Si atom in the bottom ring. The Si−O3 bond is the weakest of the four Si−O bonds because of the strong coordination of O3 to the La^{3+} ion. This activates the Si atom to a sufficient extent to start a dealumination pathway with the assistance of the REY2 site (but not sufficient to adsorb a water molecule on the Si atom directly). A water molecule sorbed on REY2 can be dissociated into a hydroxyl that moves to the Si atom and a proton that moves to O1(−Si) with a barrier of +24.2 kcal/mol (Figure 11). This removes the formal negative charge on

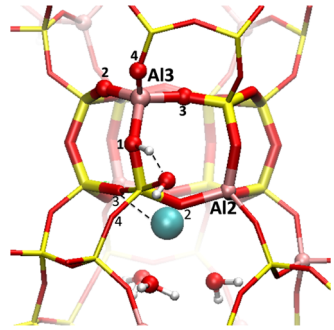

Figure 11. REY3-(SiW)-WP1 TS. The Si atom between Al2 and Al3 is a weak Lewis acid, as a result of which the incoming water molecule dissociates there.

the REY3 site, which can now sorb a water molecule. The minimum energy dealumination pathway resulting from this initial state has an activation barrier of 23.7 kcal/mol, so the initial barrier of 24.2 kcal/mol to create the initial state is the rate-limiting step. Again, the details for this route can be found in the Supporting Information. The activation barrier of 24.2 for this route is the lowest found for dealumination of REY3 and is compared to the HY3 pathway in Figure 12.

■ ROLE OF RE

Table 6 provides the activation energies for the minimum energy pathways for all sites. It is clear that for each of the sites, the incorporation of the La^{3+} ion increases the activation

https://dx.doi.org/10.1021/acs.jpcc.9b11956
J. Phys. Chem. C 2020, 124, 4626−4636

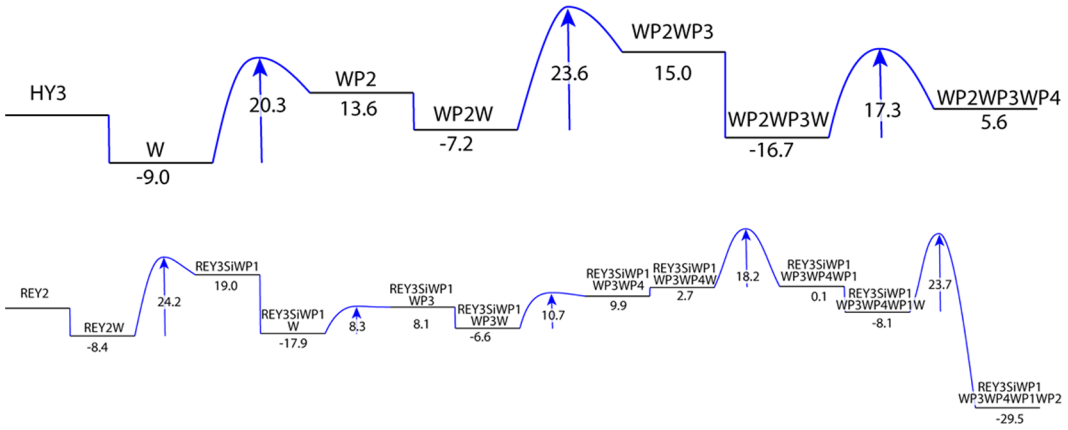

Figure 12. Minimum energy pathway for the dealumination of REY2 (starting from water adsorption on REY2) compared to the dealumination pathway of HY3. The activation barrier for the REY3 pathway is 0.6 kcal/mol higher than the HY3 pathway.

Table 6. Activation Energies for the Minimum Energy Pathways for All Sites

	HY	REY
single	24.1	n.a.
site 1	19.7	24.0
site 2	21.9	26.0
site 3	23.6	24.2

barrier for dealumination. This even holds for site 3, for which the value would have been much higher if the kick-start by REY2 would not have been available.

Although we realize that the three sites examined here are a subset of the full 12 that are available in the zeolite model, we believe that our computational evidence supports the notion that the introduction of RE in the zeolite lattice directly influences the energetics of the dealumination pathways to such an extent that stabilization of the lattice can be expected.

CONCLUSIONS

We have examined the dealumination pathways of Y-zeolites with two different Al concentrations in the absence and presence of La^{3+} ions. We conclude that the Al distribution found experimentally for a zeolite with Si/Al = 3 does not represent the thermodynamically most stable distribution. In the search for the global minimum energy structure, different counterions lead to different Al distributions, which implies that the stability of the lattice depends on the (hardness of the) counterions present. Since the aluminum distribution in this type of zeolite is likely not determined thermodynamically, we introduce a new model, with a distribution that optimally matches literature NMR data. We report that the dealumination pathways in the presence of La^{3+} all have a higher activation energy than the pathways in the absence of La^{3+}. This supports the observed stabilizing effect of hydrated La^{3+} on the dealumination. The local environment (OH groups, hydrogen bonds) has a strong effect on the dealumination pathways. Protonation of oxygen atoms close to other Brønsted acid sites is disfavored, while alternative barriers are often brought down via coordination of Al−OH groups to neighboring Lewis acid sites. This demonstrates that full periodic calculations with realistic aluminum distributions must be employed in this type of study.

ASSOCIATED CONTENT

Supporting Information

The Supporting Information is available free of charge at https://pubs.acs.org/doi/10.1021/acs.jpcc.9b11956.

Detailed information on the lanthanum benchmark, detailed information on the aluminum placing and the resulting model, an illustration of the dealumination pathway for the HY sample, additional images related to the other pathways, and full schemes and energetics for all routes (PDF)

CP2K input file for one of the steps, detailing the choices made, as well as the transition-state search method (TXT)

CIF files for all of the structures depicted in the figures both in the main text (ZIP)

AUTHOR INFORMATION

Corresponding Author

Eelco T. C. Vogt − *Albemarle Catalysts Company BV, 1022 AB Amsterdam, The Netherlands; Inorganic Chemistry and Catalysis Group, Debye Institute for Nanomaterials Science, Utrecht University, 3584 CG Utrecht, The Netherlands;* orcid.org/0000-0003-4556-4283; Email: e.t.c.vogt@uu.nl, eelco.vogt@albemarle.com

Authors

Jaap N. Louwen − *Albemarle Catalysts Company BV, 1022 AB Amsterdam, The Netherlands*

Stanislav Simko − *Inorganic Chemistry and Catalysis Group, Debye Institute for Nanomaterials Science, Utrecht University, 3584 CG Utrecht, The Netherlands*

Katarina Stanciakova − *Inorganic Chemistry and Catalysis Group, Debye Institute for Nanomaterials Science, Utrecht University, 3584 CG Utrecht, The Netherlands*

Rosa E. Bulo − *Inorganic Chemistry and Catalysis Group, Debye Institute for Nanomaterials Science, Utrecht University, 3584 CG Utrecht, The Netherlands*

Bert M. Weckhuysen − *Inorganic Chemistry and Catalysis Group, Debye Institute for Nanomaterials Science, Utrecht University, 3584 CG Utrecht, The Netherlands;* orcid.org/0000-0001-5245-1426

Complete contact information is available at: https://pubs.acs.org/10.1021/acs.jpcc.9b11956

https://dx.doi.org/10.1021/acs.jpcc.9b11956
J. Phys. Chem. C 2020, 124, 4626−4636

Author Contributions

The manuscript was written through contributions of all authors. All authors have given approval to the final version of the manuscript.

Notes

The authors declare no competing financial interest.

■ ACKNOWLEDGMENTS

The authors acknowledge funding in the form of computer-time from the Distributed European Computing Initiative (DECI)-14 program from the Partnership for Advanced Computing in Europe (PRACE). The results of this research have been achieved using the DECI resource Fionn based in Ireland at ICHEC with support from the PRACE aisbl. This work was further supported by the Netherlands Center for Multiscale Catalytic Energy Conversion (MCEC), an NWO Gravitation program funded by the Netherlands Ministry of Education, Culture and Science.

■ REFERENCES

(1) Vogt, E. T. C.; Weckhuysen, B. M. Fluid Catalytic Cracking: Recent Developments on the Grand Old Lady of Zeolite Catalysis. *Chem. Soc. Rev.* **2015**, *44*, 7342−7370.
(2) Breck, D. W. Crystalline Zeolite Y. US3,130,007A, 1964.
(3) Plank, C. J.; Rosinski, E. J.; Hawthorne, W. P. Acidic Crystalline Aluminosilicates. *Ind. Eng. Chem. Prod. Res. Dev.* **1964**, *3*, 165−169.
(4) Li, C.-Y.; Rees, L. V. C. The Thermal Stability of Faujasites with Different Si/AI Ratios. *Zeolites* **1986**, *6*, 60−65.
(5) Rabo, J.; Angell, C.; Schomaker, V. In *Catalytic and Structural Properties or Rare-Earth Exchanged Forms of Type Y Zeolites*, The IVth International Congress on Catalysis, Moscow, 1968; pp 966−993.
(6) Lee, E. F. T.; Rees, L. V. C. Effect of Calcination on Location and Valency of Lanthanum Ions in Zeolite Y. *Zeolites* **1987**, *7*, 143−147.
(7) Breck, D. W.; Flanigen, E. M. Synthesis and Properties of Union Carbide Zeolites L, X, and Y. In *Molecular Sieves*; Barrer, R. M., Ed.; Society of Chemical Industry: London, 1968; pp 47−61.
(8) Roelofsen, J. W.; Mathies, H.; de Groot, R.; van Woerkom, P.; Angad Gaur, H. Effect of Rare Earth Loading in Y-Zeolite on Its Dealumination during Thermal Treatment. *Stud. Surf. Sci. Catal.* **1986**, *28*, 337−344.
(9) van Bokhoven, J. A.; Roest, A. L.; Koningsberger, D. C.; Miller, J. T.; Nachtegaal, G. H.; Kentgens, A. P. M. Changes in Structural and Electronic Properties of the Zeolite Framework Induced by Extraframework Al and La in H-USY and La (x) NaY: A ^{29}Si and ^{27}Al MAS NMR. *J. Phys. Chem. B* **2000**, *104*, 6743−6754.
(10) Schüßler, F.; Pidko, E.; Kolvenbach, R.; Sievers, C.; Hensen, E.; van Santen, R. A.; Lercher, J. A. Nature and Location of Cationic Lanthanum Species in High Alumina Containing Faujasite Type Zeolites. *J. Phys. Chem. C* **2011**, *115*, 21763−21776.
(11) Noda, T.; Suzuki, K.; Katada, N.; Niwa, M. Combined Study of IRMS-TPD Measurement and DFT Calculation on Brønsted Acidity and Catalytic Cracking Activity of Cation-Exchanged Y Zeolites. *J. Catal.* **2008**, *259*, 203−210.
(12) Silaghi, M.-C.; Chizallet, C.; Sauer, J.; Raybaud, P. Dealumination Mechanisms of Zeolites and Extra-Framework Aluminum Confinement. *J. Catal.* **2016**, *339*, 242−255.
(13) Hutter, J.; Iannuzzi, M.; Schiffmann, F.; VandeVondele, J. CP2K: Atomistic Simulations of Condensed Matter Systems. *Wiley Interdiscip. Rev.: Comput. Mol. Sci.* **2014**, *4*, 15−25.
(14) Borštnik, U.; Vandevondele, J.; Weber, V.; Hutter, J. Sparse Matrix Multiplication: The Distributed Block-Compressed Sparse Row Library. *Parallel Comput.* **2014**, *40*, 47−58.
(15) Vandevondele, J.; Krack, M.; Mohamed, F.; Parrinello, M.; Chassaing, T.; Hutter, J. Quickstep: Fast and Accurate Density Functional Calculations Using a Mixed Gaussian and Plane Waves Approach. *Comput. Phys. Commun.* **2005**, *167*, 103−128.
(16) VandeVondele, J.; Hutter, J. An Efficient Orbital Transformation Method for Electronic Structure Calculations. *J. Chem. Phys.* **2003**, *118*, 4365−4369.
(17) Lippert, G.; Hutter, J.; Parrinello, M. A Hybrid Gaussian and Plane Wave Density Functional Scheme. *Mol. Phys.* **1997**, *92*, 477−488.
(18) Perdew, J. P.; Burke, K.; Ernzerhof, M. Generalized Gradient Approximation Made Simple. *Phys. Rev. Lett.* **1996**, *77*, 3865−3868.
(19) VandeVondele, J.; Hutter, J. Gaussian Basis Sets for Accurate Calculations on Molecular Systems in Gas and Condensed Phases. *J. Chem. Phys.* **2007**, *127*, No. 114105.
(20) Goedecker, S.; Teter, M.; Hutter, J. Separable Dual-Space Gaussian Pseudopotentials. *Phys. Rev. B* **1996**, *54*, 1703−1710.
(21) Hartwigsen, C.; Goedecker, S.; Hutter, J. Relativistic Separable Dual-Space Gaussian Pseudopotentials from H to Rn. *Phys. Rev. B: Condens. Matter Mater. Phys.* **1998**, *58*, 3641−3662.
(22) Krack, M. Pseudopotentials for H to Kr Optimized for Gradient-Corrected Exchange-Correlation Functionals. *Theor. Chem. Acc.* **2005**, *114*, 145−152.
(23) Stanciakova, K.; Ensing, B.; Göltl, F.; Bulo, R. E.; Weckhuysen, B. M. Cooperative Role of Water Molecules during the Initial Stage of Water-Induced Zeolite Dealumination. *ACS Catal.* **2019**, 5119−5135.
(24) Frigo, M.; Johnson, S. G. The Design and Implementation of FFTW3. *Proc. IEEE* **2005**, *93*, 216−231.
(25) Ling, S. GTH Basis Set Generation for Lanthanide ions-cp2k https://groups.google.com/forum/#!topic/cp2k/LZLSBQUPna8 (accessed Dec 26, 2019).
(26) Henkelman, G.; Jónsson, H. A Dimer Method for Finding Saddle Points on High Dimensional Potential Surfaces Using Only First Derivatives. *J. Chem. Phys.* **1999**, *111*, 7010−7022.
(27) Henkelman, G.; Uberuaga, B. P.; Jónsson, H. Climbing Image Nudged Elastic Band Method for Finding Saddle Points and Minimum Energy Paths. *J. Chem. Phys.* **2000**, *113*, 9901−9904.
(28) Kresse, G.; Furthmüller, J. Efficient Iterative Schemes for Ab Initio Total-Energy Calculations Using a Plane-Wave Basis Set. *Phys. Rev. B: Condens. Matter Mater. Phys.* **1996**, *54*, 11169−11186.
(29) Giannozzi, P.; Baroni, S.; Bonini, N.; Calandra, M.; Car, R.; Cavazzoni, C.; Ceresoli, D.; Chiarotti, G. L.; Cococcioni, M.; Dabo, I.; et al. QUANTUM ESPRESSO: A Modular and Open-Source Software Project for Quantum Simulations of Materials. *J. Phys.: Condens. Matter* **2009**, *21*, No. 395502.
(30) Philipsen, P. H. T.; te Velde, G.; Baerends, E. J.; Berger, J. A.; de Boeij, P. L.; Groeneveld, J. A.; Kadantsev, E. S.; Klooster, R.; Kootstra, F.; Romaniello, P. et al. *BAND. SCM, Theoretical Chemistry, Free University of Amsterdam*; Amsterdam, The Netherlands.
(31) Te Velde, G.; Baerends, E. J. Precise Density-Functional Method for Periodic Structures. *Phys. Rev. B* **1991**, *44*, 7888−7903.
(32) Wiesenekker, G.; Baerends, E. J. Quadratic Integration over the Three-Dimensional Brillouin Zone. *J. Phys. Condens. Matter* **1991**, *3*, 6721−6742.
(33) Franchini, M.; Philipsen, P. H. T.; Visscher, L. The Becke Fuzzy Cells Integration Scheme in the Amsterdam Density Functional Program Suite. *J. Comput. Chem.* **2013**, *34*, 1819−1827.
(34) Franchini, M.; Philipsen, P. H. T.; van Lenthe, E.; Visscher, L. Accurate Coulomb Potentials for Periodic and Molecular Systems through Density Fitting. *J. Chem. Theory Comput.* **2014**, *10*, 1994−2004.
(35) Saunders, V. R.; Dovesi, R.; Roetti, C.; Orlando, R.; Zicovich-Wilson, C. M.; Harrison, N. M.; Doll, K.; Civalleri, B.; Bush, I.; D'Arco, P. et al. *CRYSTAL2003 User's Manual*; University of Turin: Turin, 2003.
(36) Clark, S. J.; Segall, M. D.; Pickard, C. J.; Hasnip, P. J.; Probert, M. I. J.; Refson, K.; Payne, M. C. First Principles Methods Using CASTEP. *Z. Kristallogr. − Cryst. Mater.* **2005**, *220*, 567−570.
(37) Schüßler, F.; Schallmoser, S.; Shi, H.; Haller, G. L.; Ember, E.; Lercher, J. A. Enhancement of Dehydrogenation and Hydride Transfer by La^{3+} Cations in Zeolites during Acid Catalyzed Alkane Reactions. *ACS Catal.* **2014**, *4*, 1743−1752.

https://dx.doi.org/10.1021/acs.jpcc.9b11956
J. Phys. Chem. C 2020, 124, 4626−4636

(38) Fichtner-Schmittler, H.; Lohse, U.; Engelhardt, G.; Patzelová, V. Unit Cell Constants of Zeolites Stabilized by Dealumination Determination of Al Content from Lattice Parameters. *Cryst. Res. Technol.* **1984**, *19*, K1−K3.
(39) Loewenstein, W. The Distribution of Aluminum in the Tetrahedra of Silicates and Aluminates. *Am. Mineral.* **1954**, *39*, 92−96.
(40) Dempsey, E. Calculation of Madelung Potentials for Faujasite-Type Zeolites. I. *J. Phys. Chem. A* **1969**, *73*, 3660−3668.
(41) Schröder, K. P.; Sauer, J. Preferred Stability of Aluminum-Oxygen-Silicon-Oxygen-Aluminum Linkages in High-Silica Zeolite Catalysts: Theoretical Predictions Contrary to Dempsey's Rule. *J. Phys. Chem. B* **1993**, *97*, 6579−6581.
(42) Catlow, C. R. A.; Cormack, A. N.; Théobald, F. Structure Prediction of Transition-metal Oxides Using Energy-minimization Techniques. *Acta Crystallogr., Sect. B: Struct. Sci.* **1984**, *40*, 195−200.
(43) Klinowski, J.; Ramdas, S.; Thomas, J. M.; Fyfe, C. A.; Hartman, J. S. A Re-Examination of Si, Al Ordering in Zeolites NaX and NaY. *J. Chem. Soc., Faraday Trans. 2* **1982**, *78*, 1025−1050.
(44) Melchior, M. T.; Vaughan, D. E. W.; Pictroski, C. F. Local Environment Fine Structure in the ^{29}Si NMR Spectra of Faujasite Zeolites. *J. Phys. Chem. C* **1995**, *99*, 6128−6144.
(45) Allu, A. R.; Gaddam, A.; Ganisetti, S.; Balaji, S.; Siegel, R.; Mather, G. C.; Fabian, M.; Pascual, M. J.; Ditaranto, N.; Milius, W.; et al. Structure and Crystallization of Alkaline-Earth Aluminosilicate Glasses: Prevention of the Alumina-Avoidance Principle. *J. Phys. Chem. B* **2018**, *122*, 4737−4747.
(46) Heard, C. J.; Grajciar, L.; Nachtigall, P. The Effect of Water on the Validity of Löwenstein's Rule. *Chem. Sci.* **2019**, *10*, 5705−5711.
(47) Fletcher, R. E.; Ling, S.; Slater, B. Violations of Löwenstein's Rule in Zeolites. *Chem. Sci.* **2017**, *8*, 7483−7491.
(48) Smith, J. V.; Bennett, J. M.; Flanigen, E. M. Dehydrated Lanthanum-Exchanged Type Y Zeolite. *Nature* **1967**, *215*, 241−244.

https://dx.doi.org/10.1021/acs.jpcc.9b11956
J. Phys. Chem. C 2020, 124, 4626−4636